Available online at www.sciencedirect.com
SCIENCE DIRECT
Journal of Molecular Catalysis A: Chemical 248 (2006) 10–16
JOURNAL OF MOLECULAR CATALYSIS A: CHEMICAL
www.elsevier.com/locate/molcata

On the kinetics of iridium nanoparticles formation in ionic liquids and olefin hydrogenation

Gledison S. Fonseca [a], Josiel B. Domingos [a], Faruk Nome [b], Jairton Dupont [a,*]

[a] *Laboratory of Molecular Catalysis, Institute of Chemistry, UFRGS Avenida Bento Gonçalves, 9500 Porto Alegre, 91501-970 RS, Brazil*
[b] *Departamento de Quúmica, Universidade Federal de Santa Catarina, Florianópolis, SC 88040-900, Brazil*

Received 17 November 2005; received in revised form 5 December 2005; accepted 6 December 2005
Available online 18 January 2006

Abstract

The in situ formation of an iridium nanoparticles dispersion obtained from the reduction of the organometallic precursor $[Ir(cod)Cl]_2$ in 1-*n*-butyl-3-methyl imidazolium hexafluorophosphate ionic liquid by molecular hydrogen is an autocatalytic process. These nanoparticles possess a small size and a monomodal size distribution of 2.0 ± 0.4 nm iridium nanoparticles can be confirmed by TEM and XRD analysis before and after the catalytic process. The 1-decene hydrogenation by the Ir(0) nanoparticles in the ionic liquid follows the classical monomolecular surface reaction mechanism $\left(v = \frac{k_c K[S]}{1+K[S]}\right)$. The reaction rate is a mass controlled process under hydrogen pressure <4 atm. The catalytic kinetic constant (k_c) and the adsorption constant (K) under hydrogen pressures ≥4 atm are independent of the hydrogen concentration indicating zero order dependence on hydrogen pressure and the reaction depends only of the 1-decene concentration in the ionic liquid.

Keywords: Ionic liquids; Nanoparticles; Iridium; Hydrogenation; Autocatalytic

1. Introduction

Without doubt the olefin hydrogenation reactions promoted by transition-metal complexes in homogeneous conditions and by classical heterogenous catalysts are one of the most investigated catalytic reactions and fundamental aspects such kinetics and mechanism are well known [1,2]. Conversely, little attention has been paid to the kinetics of the hydrogenation reactions catalyzed by soluble transition-metal nanoparticles in one-phase and multiphase conditions [3–8]. The recent advent in metal nanoparticles synthetic control methods has resulted in a new impulse on the synthesis and applications of soluble transition-metal nanoparticles in catalysis, particularly for hydrogenation and C–C coupling reactions [4,9–14]. In this respect, it is expected that soluble transition-metal nanoparticles of 1–10 nm in size will exhibit physical–chemical properties intermediate between those of the smallest element from which they can be composed and those of the bulk material [15,16]. Indeed, in many cases this new generation of soluble nanoparticles gave singular catalytic activities/selectivities i.e. different from that expected for a molecular (single-site) or heterogeneous catalysts (multi-site) [17,18]. However, in other cases these nanoparticles behaves like classical heterogeneous catalysts [19–28] and in some other cases these soluble materials are decomposed, under the reaction conditions, generating monometallic homogenous catalytic active species [29].

We have recently demonstrated that Ir(0) nanoparticles prepared in 1-*n*-butyl-3-methylimidazolium hexafluorophosphate ionic liquid had a small size and monomodal distribution and are stable and active catalysts for the hydrogenation of alkenes and arenes in multiphase conditions [30,31]. We now report the kinetic model for the hydrogenation of olefins by these nanoparticles dispersed in the ionic liquid.

2. Results and discussion

The in situ reduction of the organometallic precursor $[Ir(cod)Cl]_2$ (cod = 1,5-cyclooctadiene) dispersed in 1-*n*-butyl-3-methylimidazolium hexafluorophosphate (BMI·PF_6) ionic liquid by molecular hydrogen has been used as catalytic system

* Corresponding author.
E-mail address: dupont@iq.ufrgs.br (J. Dupont).

1381-1169/$ – see front matter © 2005 Elsevier B.V. All rights reserved.
doi:10.1016/j.molcata.2005.12.002

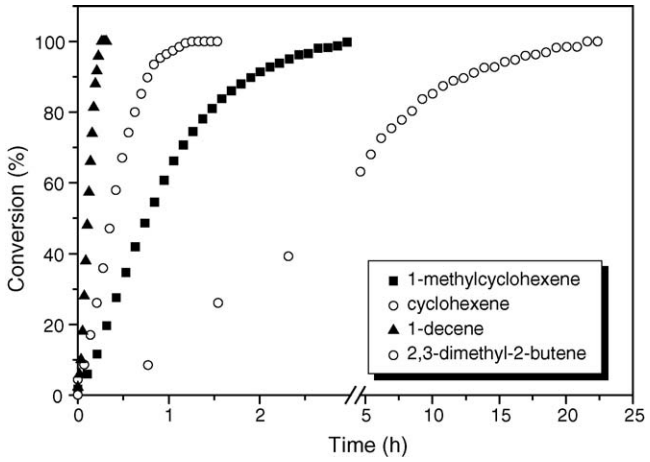

Fig. 1. Hydrogenation of olefins catalyzed by in situ iridium nanoparticles dispersed in BMI·PF_6 (1 mL) at 4 atm constant hydrogen pressure (constant pressure) at 75 °C.

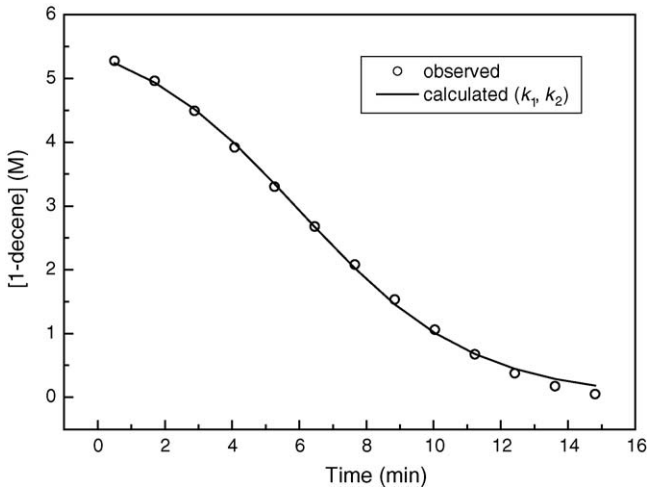

Fig. 2. Hydrogenation curve fits for 1-decene hydrogenation with the catalyst precursor $[Ir(cod)Cl]_2$ dispersed in BMI·PF_6 (1 mL), 4 atm constant hydrogen pressure at 75 °C. The solid line is the curve fitting using the two steps [A → B, A + B → 2B (k_1, k_2)] mechanism. The 1-decene/Ir molar ratio is 1215.

for the hydrogenation reaction of di-, tri- and tetra-substituted olefins and the obtained results are shown in Fig. 1. These results show that there is a strong dependence of the rate of hydrogenation on the structure of the alkene and the observed rate constants decrease in the order 1-decene > cyclohexene > 1-methylcyclohexene > 2,3-dimethyl-2-butene, a reactivity order clearly related with the increase in steric demand of the non-linear substituted alkenes. Similar trend is characteristic of classical homogenous catalysts such as $[Ir(cod)(P\ ^{i}Pr_3)(py)]PF_6$ [32]. Noteworthy, the isolated and re-dispersed nanoparticles in the ionic liquids gave the same results for the catalytic hydrogenation reactions.

In all cases, hydrogenation by $[Ir(cod)Cl]_2$ dispersed in BMI·PF_6 (1 mL) ionic liquid has a typical sigmoidal shape with very short induction periods. This kinetic behavior is characteristic of an autocatalytic mechanism and a strong indication of transition metal nanoclusters formation under hydrogen [33]. These experimental curves, as for example for the 1-decene hydrogenation (Fig. 2), can be fitted to the autocatalytic kinetic model that can involve basically: nucleation (A → B, k_1) and autocatalytic surface growth (A + B → 2B, k_2) [33]. The obtained values for the nucleation and autocatalytic growth constants, from the fit of Fig. 2, k_1 and k_2 are 2.04 h^{-1} and 5125 $M^{-1}\,h^{-1}$, respectively. Moreover, attempts to fit the curve with a mechanism including a third step, the bimolecular aggregation (B + B → C, k_3) [34,35], or with the recently discovered double autocatalytic mechanism [36,37], which includes a fourth step for the formation of bulk-metal (B + C → 1.5C, k_4), did not converge the fit, which strongly suggests that agglomeration is not significant in this case.

Indeed, TEM analysis (Fig. 3) of the nanoparticles dispersed in BMI·PF_6 before and after catalysis show no sign of agglomeration (2.0 ± 0.4 nm), indicating that the ionic liquid promote a fundamental stabilization of the nanoparticles at the nucleation step, resulting in particles with a very small size and a monomodal distribution. In addition, XRD analysis shows the presence of broad reflection lines indicating the diffraction by very small crystals. The four diffractions peaks were assigned as correspond to the Ir(0) (1 1 1), (2 0 0), (2 2 0) and (3 1 1) reflection planes. The most representative reflections of Ir(0) were indexed as a face-centered cube (fcc) with unit cell parameter $a = 3.8784$. The calculated (using the Scherrer equation) mean diameter of Ir(0) nanoparticles before and after catalysis are 2.1 and 2.3 nm, respectively.

The influence of the substrate/catalyst concentration ratio, hydrogen pressure and reaction temperature has been investigated for the 1-decene hydrogenation. The results obtained with different catalyst precursor concentrations on the 1-decene hydrogenation by the Ir(0) nanoparticles in BMI·PF_6 are presented in Table 1 and Fig. 4. The results show clearly that at a substrate/catalyst ratio of ca. 5000 catalyst saturation occurs, i.e., starting from this "substrate/catalyst concentration ratio", the frequency turnover (TOF) remains constant. This result suggests that a very important limiting factor of the hydrogenation reaction is the miscibility of 1-decene in the ionic liquid that is around 1.4 mol% at room temperature [38]. Noteworthy that diffusion of reactants is a common rate-determining factor in a variety of reactions and sorption processes performed under multiphase conditions.

Table 1
Influence of the 1-decene/Ir ratio on the catalytic activity for the 1-decene hydrogenation by Ir(0) nanoparticles in BMI·PF_6 (1 mL) at 75 °C and 4 atm of hydrogen (constant pressure)

Entry	Olefin/Ir	Time (h)[a]	TOF (h^{-1})[b]
1	1215	0.30	4050 (7776)
2	2430	0.33	7363 (14137)
3	4937	0.33	14960 (28723)
4	6583	0.66	9974 (19150)
5	9875	1.33	7425 (14256)
6	19750	1.83	10800 (20736)

[a] Time for 100% of 1-decene conversion.
[b] Turnover frequency mol(1-decene)/mol($[Ir(cod)Cl]_2$) h and in parenthesis the corrected turnover frequency (by means of magic-number approach [39]) considering only the exposed atoms on the nanoparticle surface (52%).

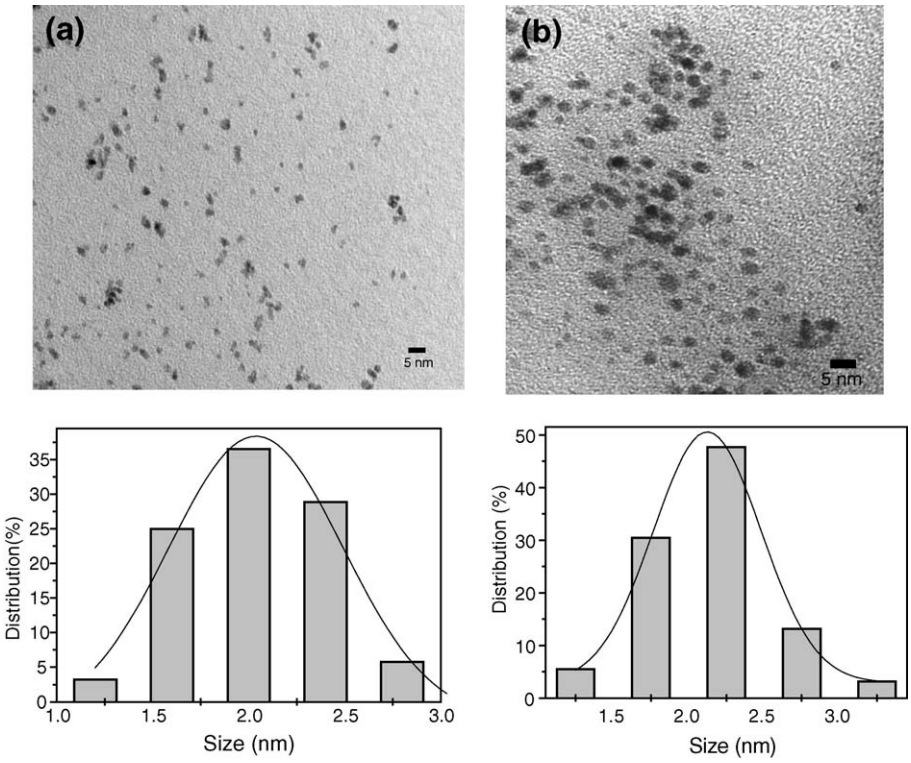

Fig. 3. Transmission electron micrograph and size distribution of the iridium nanoparticles in BMI·PF_6 (a) before and (b) after hydrogenation of 1-decene.

Fixing the substrate/catalyst ratio at S/C = 4937, the effect of the increase in hydrogen pressure of the system was investigated and the experimental results are shown in Fig. 5 and summarized in Table 2.

Fig. 5 shows the initial conversion rate (the induction time period is not used) as a function of hydrogen pressure. It is clear from the data in Fig. 5 that increasing the hydrogen pressure causes an augmentation on the reaction rate until saturation. This rate saturation effect as a function of hydrogen pressure most probably indicates that the surface of the nanoparticles is already saturating from 4 atm of pressure. Although saturation of weakly interacting systems is not expected, since basically they should obey Henry's law, the increase in solubility in the ionic liquid will certainly result in the saturation of the surface of the nanoparticles, which most probably interact strongly with hydrogen. Thus, a limiting rate at high pressure is a very strong indication that the hydrogenation reaction occurs within the ionic liquid at the surface of the catalytic nanoparticles.

Similarly, it is well known that increasing the temperature in homogeneous hydrogenation and oxidation reactions, results in

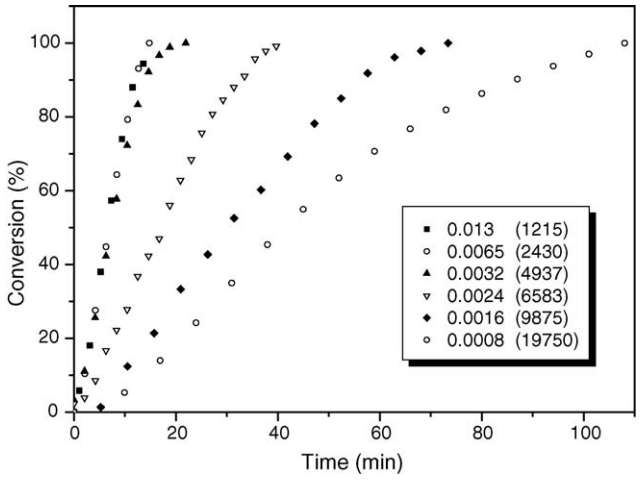

Fig. 4. 1-Decene conversion under hydrogen (4 atm, constant pressure) at room temperatures with different Ir(0) nanoparticles concentrations in BMI·PF_6 (1 mL).

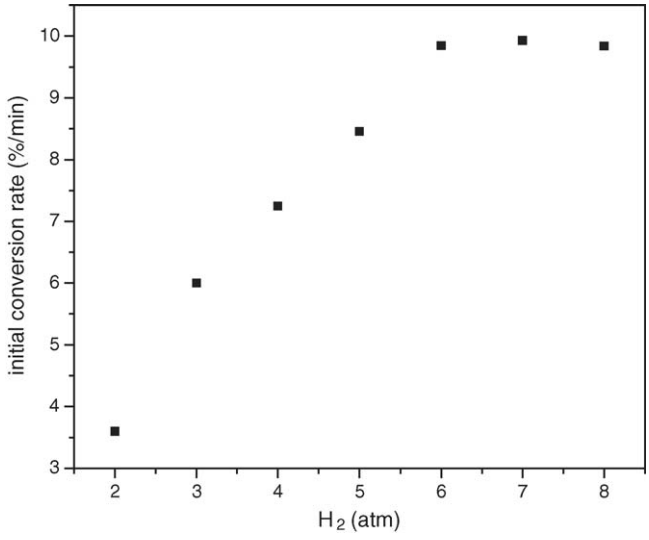

Fig. 5. Influence of the hydrogen pressure (constant pressure) on the 1-decene conversion at 75 °C by Ir(0) nanoparticles (1-decene/Ir = 4937) in BMI·PF_6 (1 mL).

Table 2
Influence of the hydrogen pressure on the catalytic activity for the 1-decene hydrogenation by Ir(0) nanoparticles in BMI·PF_6 (1 mL) at 75 °C (1-decene/Ir = 4937)

Entry	Pressure H_2 (atm)	Time (h)[a]	TOF (h^{-1})[b]
1	2	0.83	5950 (11424)
2	3	0.43	11481 (22043)
3	4	0.21	23509 (45137)
4	5	0.25	19784 (37985)
5	6	0.31	15925 (30576)
6	7	0.20	24685 (47395)
7	8	0.18	27428 (52661)

[a] Time for 100% of 1-decene conversion.
[b] Turnover frequency mol(1-decene)/mol([Ir(cod)Cl]$_2$) h and in parenthesis the corrected turnover frequency considering only the exposed atoms on the nanoparticle surface (52%).

a reaction rate increase until a limit and then the reaction rate decreases due to the contribution of the higher entropy of the gas which results in its expulsion from the solution. This behavior is also operative in the hydrogenation of 1-decene by the Ir(0) nanoparticles dissolved in BMI·PF_6 as observed on the influence of temperature on the reaction rate (Fig. 6). It is clear that the reaction is very slow at 50 °C and the rate of the reaction, calculated from the slopes of the data shown in Fig. 6, obtained at 75 and 90 °C is essentially identical within limits of experimental error (0.35 and 0.34 M min^{-1}, respectively). The experimental results suggest that diffusional parameters related to the solubilization of 1-decene in the ionic liquid and structural restrictions related to the steric demand of the alkene are the limiting parameters for the global rate reaction. The effect of temperature in the kinetics of this particular reaction is complex and does not follow a typical Arrhenius behavior. Indeed, upon an increase in temperature it is expected that the 1-decene solubility in the ionic liquid increase, but the augmentation on temperature also causes the expulsion of the hydrogen dissolved in the ionic liquid, leading to a complex kinetic profile and eventually to a decrease on the global reaction rate.

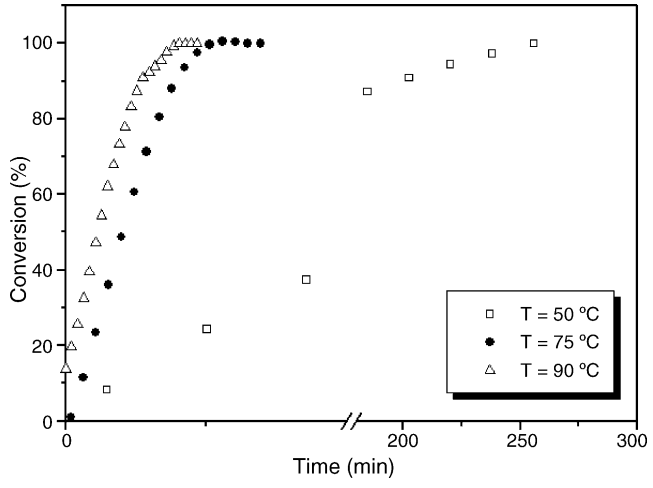

Fig. 6. Influence of the reaction temperature on the 1-decene conversion by Ir(0) nanoparticles in BMI·PF_6 (1 mL, 1-decene/Ir = 4937) at 75 °C and 4 atm of hydrogen (constant pressure).

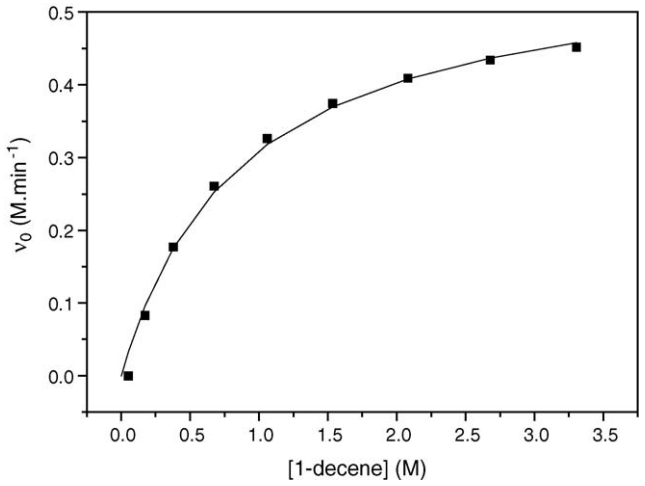

Fig. 7. Variation of v_0 with concentration of substrate for 1-decene hydrogenation by Ir(0) nanoparticles in BMI·PF_6 (1 mL) at 5 atm of molecular hydrogen and 75 °C.

Fig. 7 shows a saturation curve of initial rate (v_0) as a function of 1-decene concentration in the hydrogenation reaction with Ir(0) nanoparticles (1-decene/Ir = 4937) at 5 atm of molecular hydrogen and 75 °C. Saturation kinetics means that as the reactant concentration increases the order of reaction changes from 1st to 0th. Such behavior can be found in a variety of homogeneous (e.g. micellar or enzymatic catalysis) or heterogeneous catalytic systems.

Assuming that our catalytic system behaves as a typical pseudo-phase, where the nanoparticles are homogeneously dispersed in the ionic liquid, the observed kinetic curve can be interpreted as resulting from a monomolecular surface reaction. Clearly, this is only possible because with hydrogen pressures >4 atm the pressure does not affect the reaction rate and the surface of the nanoparticles are already saturated. In a normal weakly interacting system, following Henry's law, the simplification would not be realistic. Thus, at high pressure, the hydrogenation reaction which occurs within the ionic liquid at the surface of the catalytic nanoparticle essentially follows the monomolecular mechanism shown in Scheme 1.

According to Scheme 1, the substrate (S) interacts with the activated catalyst (C) to form the adsorbed species (SC) which undergoes reaction to form the final product (P). The rate for sorption and desorption of the substrate from the surface of the nanoparticles is given by Eqs. (1) and (2):

$$r_{ads} = k_{a1}[S](1 - \theta) \quad (1)$$

$$r_{ads} = k_{a-1}\theta \quad (2)$$

where θ is the fraction of the nanoparticles surface covered by the substrate (S). Following a single-site model for the sorption of the substrate at the surface of the catalytic nanoparticles,

$$S + C \underset{k_{a-1}}{\overset{k_{a1}}{\rightleftharpoons}} SC \xrightarrow{k_c} P$$

Scheme 1.

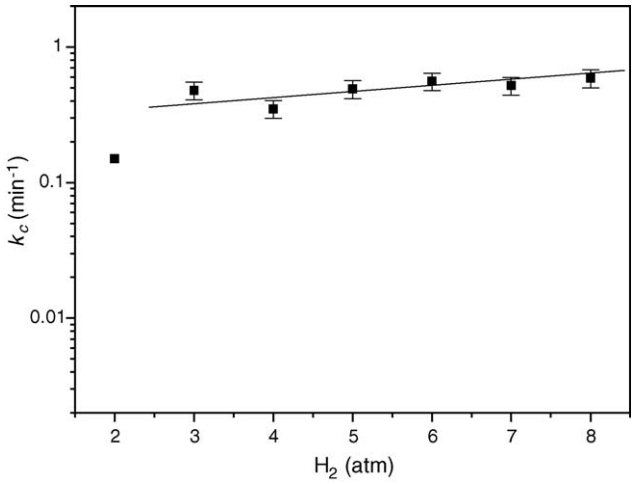

Fig. 8. Influence of the hydrogen pressure on k_c of the 1-decene hydrogenation by Ir(0) nanoparticles (1-decene/Ir = 4937) in BMI·PF_6 (1 mL).

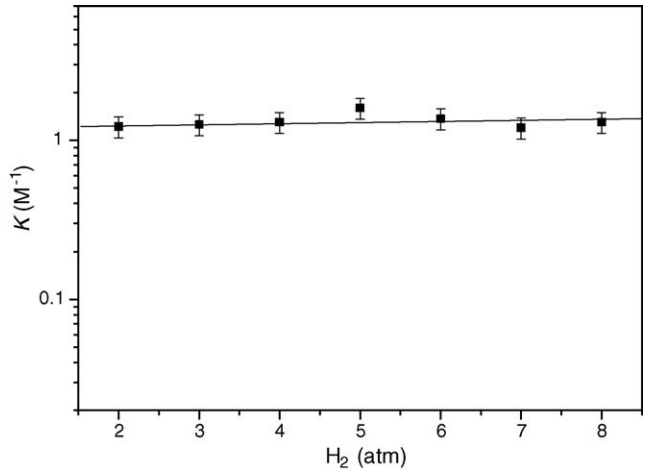

Fig. 9. Influence of the hydrogen pressure on K of the 1-decene hydrogenation by Ir(0) nanoparticles (1-decene/Ir = 4937) in BMI·PF_6 (3 mL).

the fraction of catalyst surface covered by the substrate can be expressed by:

$$\theta = \frac{K[S]}{1 + K[S]} \tag{3}$$

where K corresponds to the adsorption constant (k_{a1}/k_{a-1}). The significant effect of the structure of the alkene shown in Fig. 1, where the rate of hydrogenation was strongly dependent on the steric demand of the non-linear substituted alkenes, is strongly indicative that in the ionic liquid phase, the reaction rate will be dependent on the fraction of catalyst surface covered by the substrate (θ). Therefore, the global reaction law can be expressed by:

$$v = k_c\theta \tag{4}$$

where k_c is the catalytic kinetic constant for the formation of the products and combining Eqs. (3) and (4) we can obtain:

$$v = \frac{k_c K[S]}{1 + K[S]} \tag{5}$$

Applying Eq. (5) to the experimental data for the 1-decene hydrogenation by Ir(0) nanoparticles dissolved in BMI·PF_6 the rate constant (k_c) and the adsorption constants (K) can be easily calculated by means of non-linear fitting procedures.

The data in Fig. 8 shows that the kinetic constant (k_c) is almost identical at pressures greater than 3 atm, considering the maximum error admitted for soluble nanoparticle catalysts. However at low hydrogen pressures (2 atm) the hydrogenation rate underwent a significant decrease. This is most probably due to the fact that the hydrogen solubility in the ionic liquid follows a mass transfer process and, under the kinetic conditions, the surface of the catalytic nanoparticles is not fully saturated. At higher hydrogen pressures, as expected, the hydrogen concentration in the ionic liquid has no influence on the reaction rate with mean value for the catalytic constants of $0.45 \pm 0.06\,\text{min}^{-1}$.

The adsorption constant (K) calculated from the data at different hydrogen pressures is shown in Fig. 9 and clearly the experimental value for the adsorption constant is independent of the hydrogen concentration even at low pressure, with an average value for the adsorption constant of $K = 1.32 \pm 0.20\,\text{M}^{-1}$ calculated for the 1-decene adsorption in the surface of the iridium nanoparticles in the ionic liquid (Fig. 7).

3. Conclusions

The reduction of $[Ir(cod)Cl]_2$ (cod = 1,5-cyclooctadiene) dispersed in 1-*n*-butyl-3-methylimidazolium hexafluorophosphate ionic liquid by molecular hydrogen results in the formation of small size iridium nanoparticles, a result corroborated by TEM and XRD analysis before and after catalysis. The small size of the nanoparticles is strongly indicative that the nucleation step is faster than the autocatalytic surface-growth of the nanoparticles and is a strong indication that the ionic liquid, a highly ordered media which is known to restrict diffusion, is promoting the fundamental stabilization at the nucleation step, allowing the formation of nanoparticles with small size and monomodal size distribution. The iridium nanoparticles in ionic liquids behave as a heterogeneous catalyst for the hydrogenation of olefins following the monomolecular surface reaction mechanism $\left(v = \frac{k_c K[S]}{1+K[S]}\right)$. The adsorption constant of the alkene ($K = 1.32 \pm 0.20\,\text{M}^{-1}$) is independent of the hydrogen concentration and the different reactivities of the substituted alkenes is directly related with the sorption process. The catalytic constant (k_c) is almost identical ($0.45 \pm 0.06\,\text{min}^{-1}$) under hydrogen pressures ≥4 atm but at low hydrogen pressures (2 atm) the hydrogenation rate underwent a significant decrease indicating that at hydrogen pressures lower than 4 atm the reaction is under a mass transfer controlled process.

4. Experimental details

4.1. General

All reactions were performed under argon atmosphere using Schlenk techniques. The substrates (Acros or Aldrich) were obtained from commercial sources and used as received. The

ionic liquids were prepared according to known procedures [40,41] dried over molecular sieves (4 Å) and their purity was checked by $AgNO_3$ test, ^1H and ^{13}C NMR, and cyclic voltametry. The water (<0.1 wt.%) and chloride (<1.4 mg/L) contents in the ionic liquids used were determined by known methods [42,43]. NMR analyses were performed on a Varian Inova 300 spectrometer. Infrared spectra were obtained on a Bomen B-102 spectrometer. GC analysis were performed in a HP-5890 Gas Chromatograph with a FID detector and 30-m capillary column with dimethylpolysiloxanes stationary phase and GC/MS Shimadzu QP-5050 (EI, 70 eV) for mass spectra analysis. The products obtained were analyzed by GC (comparison with the retention times of authentic samples) and characterized by GC/MS, IR, ^1H and ^{13}C NMR. All hydrogenation reactions were performed on a modified Fischer–Porter reactor immersed in a silicon oil bath and connected to a hydrogen tank. The system temperature was kept at 75 °C under constant stirring (800 rpm). The fall in the hydrogen pressure in the tank was monitored with a pressure transducer interfaced through a Novus converter to a PC and the data workup via Microcal Origin 5.0. The kinetic data for 1-decene hydrogenation were fit using an analytic expression with Microcal Origin 5.0. The kinetic data for 1-decene hydrogenation were fit using an analytic expression with Microcal Origin 5.0 (for k_1 and k_2) or the MacKinetics v. 0.9.1b numerical integration (for k_1, k_2 and k_3). The actual rate constants obtained from the fitting for the autocatalytic growth ($A + B \rightarrow 2B$, k_{2obs}) and agglomeration ($B + B \rightarrow C$, k_{3obs}) steps were corrected considering the reaction stoichiometry (substrate/catalyst molar ratio), to obtain the reported rate constants, k_2 and k_3 (for further details on these fitting procedures see elsewhere) [34,35,37,44].

4.2. General procedure for the 1-decene hydrogenation

The organometallic precursor $[Ir(cod)Cl]_2$ (16 mg, 0.05 mmol) was dissolved in dichloromethane (3 mL) and mixed with 1 mL of ionic liquid ($BMI{\cdot}PF_6$). This yellow solution was stirred at room temperature for 15 min and the volatiles were removed under vacuum at 75 °C for 20 min. The 1-decene (1.02 g, 7.3 mmol) was added and 4 bar of molecular hydrogen was admitted to the system. The fall in the hydrogen pressure in the tank was monitored with a pressure transducer interfaced through a Novus converter to a PC and the data workup via Microcal Origin 5.0. The organic phase was analyzed by GC/MS.

4.3. Synthesis of iridium nanoparticles

In Fischer–Porter Bottle containing an yellow solution of the organometallic precursor $[Ir(cod)Cl]_2$ (4 mg, 0.006 mmol) in dichloromethane (3 mL) was added to 1 mL of the ionic liquid, and stirred at room temperature for 15 min. The volatiles were then removed under reduced pressure (0.1 bar) at 75 °C for 20 min. The system was maintained at 75 °C and hydrogen (4 bar) was admitted to the system. After stirring for 10 min, a black "solution" was obtained and one part were analyzed by TEM and the other part was diluted in acetone (5 mL) and isolated by centrifugation (3000 rpm) for 5 min and washed with acetone (3× 5 mL) and dried under reduced pressure and analyzed by XRD.

4.4. XRD analysis

For the XRD analyses the nanoparticles were isolated as a fine powder and placed in the sample holder. The wide angle X-ray diffraction (WAXD) experiments were carried out on a SIEMENS D500 diffractometer equipped with curved graphite crystal using Cu Kα radiation ($\lambda = 1.5406$ Å). The diffraction data were collected at room temperature in a Bragg–Brentano $\theta - 2\theta$ geometry. The equipment was operated at 40 kV and 20 mA with a scan range between 10° and 100°. The diffractograms were obtained with a constant step, $\Delta 2\theta = 0.05$. The indexation of Bragg reflections was obtained by a pseudo-voigt profile fitting using the FULLPROF code. XRD shows the presence of broad reflection lines indicating the diffraction by very small crystals. The four diffractions peaks were assigned as correspond to the Ir(0) (1 1 1), (2 0 0), (2 2 0) and (3 1 1) reflection planes. The most representative reflections of Ir(0) were indexed as a face-centered cube (fcc) with unit cell parameter $a = 3.8784$. The calculated (using the Scherrer equation) mean diameter of Ir(0) nanoparticles before and after catalysis are 2.1 and 2.3 nm, respectively.

4.5. TEM analysis

The morphologies and the electron diffraction (ED) of the obtained particles were carried out on a JEOL JEM–2010 equipped with an energy dispersive X-ray spectroscopy (EDS) system and JEOL JEM–1200 EXII electron microscope operating at an accelerating voltage of 200 and 120 kV, respectively. The samples for TEM were prepared by deposition of the Iridium nanoparticles in ionic liquids at room temperature on a carbon-coated copper grid. The histograms of the nanoparticles size distribution were obtained from measurement of around 300–350 particles, and were reproduced in different regions of the Cu grid, assuming spherical shape, found in an arbitrary chosen area of enlarged micrographs.

Acknowledgements

Thanks are due to the following Brazilian agencies: CNPq, CAPES and CT-PETRO for partial financial support. We also acknowledge the staff of LNLS (Project D11A-SAXS, 2003) for the technical assistance and Dr. Giovanna Machado for the XRD and TEM analysis. We also thank Prof. R.G. Finke and E.E. Finney (Colorado State University) for the help in the curves fitting and in the use of MacKinetic program.

References

[1] I. Chorkendorff, J.W. Niemantsverdriet, Concepts of Modern Catalysis and Kinetics, 1st ed., Wiley–VCH, Weinheim, 2003.
[2] R.A. Van Santen, P.W.N.M. Van Leeuwen, J.A. Moulijn, B.A. Averill (Eds.), Stud. Surf. Sci. Catal., vol. 123, 2nd Revised and Enlarged ed., Elsevier, Amsterdan, 1999.

[3] L.N. Lewis, Chem. Rev. 93 (1993) 2693.
[4] A. Roucoux, J. Schulz, H. Patin, Chem. Rev. 102 (2002) 3757.
[5] H. Bonnemann, R.M. Richards, Eur. J. Inorg. Chem. (2001) 2455.
[6] N. Toshima, Y. Shiraishi, T. Teranishi, M. Miyake, T. Tominaga, H. Watanabe, W. Brijoux, H. Bonnemann, G. Schmid, Appl. Organomet. Chem. 15 (2001) 178.
[7] J.D. Aiken, R.G. Finke, J. Mol. Catal. A: Chem. 145 (1999) 1.
[8] J.A. Widegren, R.G. Finke, J. Mol. Catal. A: Chem. 191 (2003) 187.
[9] A.K. Verma, R. Kumar, P. Chaudhary, A. Saxena, R. Shankar, S. Mozumdar, R. Chandra, Tetrahedron Lett. 46 (2005) 5229.
[10] C.A. Stowell, B.A. Korgel, Nano Lett. 5 (2005) 1203.
[11] B.D. Fitchett, J.B. Rollins, J.C. Conboy, J. Electrochem. Soc. 152 (2005) E251.
[12] V. Calo, A. Nacci, A. Monopoli, F. Montingelli, J. Org. Chem. 70 (2005) 6040.
[13] D.G. Archer, J.A. Widegren, D.R. Kirklin, J.W. Magee, J. Chem. Eng. Data 50 (2005) 1484.
[14] X.D. Mu, J.Q. Meng, Z.C. Li, Y. Kou, J. Am. Chem. Soc. 127 (2005) 9694.
[15] A.T. Bell, Science 299 (2003) 1688.
[16] D.R. Rolison, Science 299 (2003) 1698.
[17] S. Jansat, M. Gomez, K. Philippot, G. Muller, E. Guiu, C. Claver, S. Castillon, B. Chaudret, J. Am. Chem. Soc. 126 (2004) 1592.
[18] M. Valden, X. Lai, D.W. Goodman, Science 281 (1998) 1647.
[19] V. Mevellec, A. Roucoux, E. Ramirez, K. Philippot, B. Chaudret, Adv. Synth. Catal. 346 (2004) 72.
[20] J.L. Pellegatta, C. Blandy, V. Colliere, R. Choukroun, B. Chaudret, P. Cheng, K. Philippot, J. Mol. Catal. A: Chem. 178 (2002) 55.
[21] L.S. Ott, M.L. Cline, M. Deetlefs, K.R. Seddon, R.G. Finke, J. Am. Chem. Soc. 127 (2005) 5758.
[22] J.D. Aiken, R.G. Finke, J. Am. Chem. Soc. 120 (1998) 9545.
[23] G.S. Fonseca, E.T. Silveira, M.A. Gelesky, J. Dupont, Adv. Synth. Catal. 347 (2005) 847.
[24] G.S. Fonseca, J.D. Scholten, J. Dupont, Synlett (2004) 1525.
[25] A. Roucoux, J. Schulz, H. Patin, Adv. Synth. Catal. 345 (2003) 222.
[26] E. Schulz, S. Levigne, A. Roucoux, H. Patin, Adv. Synth. Catal. 344 (2002) 266.
[27] J. Schulz, A. Roucoux, H. Patin, Chem. Commun. (1999) 535.
[28] J. Schulz, A. Roucoux, H. Patin, Chem. Eur. J. 6 (2000) 618.
[29] C.C. Cassol, A.P. Umpierre, G. Machado, S.I. Wolke, J. Dupont, J. Am. Chem. Soc. 127 (2005) 3298.
[30] G.S. Fonseca, A.P. Umpierre, P.F.P. Fichtner, S.R. Teixeira, J. Dupont, Chem. Eur. J. 9 (2003) 3263.
[31] J. Dupont, G.S. Fonseca, A.P. Umpierre, P.F.P. Fichtner, S.R. Teixeira, J. Am. Chem. Soc. 124 (2002) 4228.
[32] R. Crabtree, Acc. Chem. Res. 12 (1979) 331.
[33] M.A. Watzky, R.G. Finke, J. Am. Chem. Soc. 119 (1997) 10382.
[34] J.A. Widegren, J.D. Aiken, S. Ozkar, R.G. Finke, Chem. Mater. 13 (2001) 312.
[35] B.J. Hornstein, R.G. Finke, Chem. Mater. 16 (2004) 139.
[36] C. Besson, E.E. Finney, R.G. Finke, J. Am. Chem. Soc. 127 (2005) 8179.
[37] C. Besson, E.E. Finney, R.G. Finke, Chem. Mater. 17 (2005) 4925.
[38] P. Wasserscheid, C.M. Gordon, C. Hilgers, M.J. Muldoon, I.R. Dunkin, Chem. Commun. (2001) 1186.
[39] B.K. Teo, H. Zhang, Metal Nanoparticles: Synthesis, Characterization and Applications, Marcel Dekker, New York, 2002.
[40] J. Dupont, P.A.Z. Suarez, C.S. Consorti, R.F. deSouza, Org. Synth. 79 (2002) 236.
[41] P.A.Z. Suarez, J.E.L. Dullius, S. Einloft, R.F. DeSouza, J. Dupont, Polyhedron 15 (1996) 1217.
[42] B.K. Sweeny, D.G. Peters, Electrochem. Commun. 3 (2001) 712.
[43] V. Gallo, P. Mastrorilli, C.F. Nobile, G. Romanazzi, G.P. Suranna, J. Chem. Soc., Dalton Trans (2002) 4339.
[44] B.J. Hornstein, R.G. Finke, Chem. Mater. 16 (2004) 3972.